Protein Science (1999), *8*:1536–1545. Cambridge University Press. Printed in the USA.

Structural studies by X-ray diffraction on metal substituted desulforedoxin, a rubredoxin-type protein

M. ARCHER,[1,2] A.L. CARVALHO,[1,2] S. TEIXEIRA,[1,2] I. MOURA,[1] J.J.G. MOURA,[1] F. RUSNAK,[3] AND M.J. ROMÃO[1,2]

[1]Departamento de Química, Centro de Química Fina e Biotecnologia, Faculdade de Ciências e Tecnologia, Universidade Nova de Lisboa, 2825-114 Caparica, Portugal
[2]Instituto de Tecnologia Química e Biológica, Apt. 127, 2780 Oeiras, Portugal
[3]Section of Hematology Research and Department of Biochemistry and Molecular Biology, Mayo Clinic and Foundation, Rochester, Minnesota 55905

(RECEIVED December 31, 1998; ACCEPTED April 2, 1999)

Abstract

Desulforedoxin (Dx), isolated from the sulfate reducing bacterium *Desulfovibrio gigas*, is a small homodimeric (2×36 amino acids) protein. Each subunit contains a high-spin iron atom tetrahedrally bound to four cysteinyl sulfur atoms, a metal center similar to that found in rubredoxin (Rd) type proteins. The simplicity of the active center in Dx and the possibility of replacing the iron by other metals make this protein an attractive case for the crystallographic analysis of metal-substituted derivatives. This study extends the relevance of Dx to the bioinorganic chemistry field and is important to obtain model compounds that can mimic the four sulfur coordination of metals in biology. Metal replacement experiments were carried out by reconstituting the apoprotein with In^{3+}, Ga^{3+}, Cd^{2+}, Hg^{2+}, and Ni^{2+} salts. The In^{3+} and Ga^{3+} derivatives are isomorphous with the iron native protein; whereas Cd^{2+}, Hg^{2+}, and Ni^{2+} substituted Dx crystallized under different experimental conditions, yielding two additional crystal morphologies; their structures were determined by the molecular replacement method. A comparison of the three-dimensional structures for all metal derivatives shows that the overall secondary and tertiary structures are maintained, while some differences in metal coordination geometry occur, namely, bond lengths and angles of the metal with the sulfur ligands. These data are discussed in terms of the entatic state theory.

Keywords: crystal structure; desulfoferrodoxin; desulforedoxin; iron–sulfur proteins; metal substitution; rubredoxin-type proteins

Desulforedoxin (Dx) is a small homodimeric (2×3.9 kDa) protein isolated from *Desulfovibrio gigas* (Moura et al., 1977). Each polypeptide chain contains one iron atom coordinated by four cysteine residues at positions 9, 12, 28, and 29, in a distorted tetrahedral arrangement and the midpoint redox potential is -35 mV. The X-ray structure of Dx (1DXG) was determined at 1.8 Å resolution by the Single Isomorphous Replacement with Anomalous Scattering (SIRAS) method using the indium substituted protein as a fully replaced derivative (Archer et al., 1995). The Dx dimer folds into an incomplete β-barrel (Fig. 1) representing a novel topology. Moreover, two-dimensional NMR methods have been used to determine the solution state structures of the Zn- and Cd-derivatives of Dx (Goodfellow et al., 1996, 1998).

Rubredoxins (Rd) are small monomeric proteins with molecular weights approximately 5–6 kDa, containing one iron atom tetrahedrally bound by four cysteine residues (Sieker et al., 1994). Rd with redox potentials in the range of -60 to 0 mV vs. NHE (Capozzi et al., 1998) is commonly assumed to be involved in electron transfer processes. It has been demonstrated that Rd can replace ferredoxin as an electron carrier in certain reactions (Lovenberg & Sobel, 1965). Furthermore, Rd from the aerobe *Pseudomonas oleovorans* (the only dimeric Rd isolated so far) was proposed to participate in the ω-hydroxylation of fatty acids and hydrocarbons by transferring electrons to an alkane hydroxylase (Peterson et al., 1967). Rd isolated from *D. gigas* represents an interesting case since, in the presence of oxygen, it was also shown to be involved in electron transfer conducing to ATP formation from the degradation of polyglucose (Santos et al., 1993; Gomes et al., 1997).

With only a single $Fe(SCys)_4$ per polypeptide chain, Rd and Dx are the simplest members of the iron–sulfur proteins. The

Reprint requests to: Maria João Romão, Departamento de Química, Centro de Química Fina e Biotecnologia, Faculdade de Ciências e Tecnologia, Universidade Nova de Lisboa, 2825-114 Caparica, Portugal; e-mail: mromao@dq.fct.unl.pt.

Abbreviations: ATP, adenosine 5′-triphosphate; CSD, Cambridge Structural Database; Dfx, desulfoferrodoxin; Dx, desulforedoxin; EDTA, ethylenediaminetetraacetic acid; MPD, 2-methyl-2,4-pentanediol; Nl, neelaredoxin; PDB, Protein Data Bank; PEG, polyethyleneglycol; RMSD, root-mean-square deviation; Rd, rubredoxin; Rr, rubrerythrin; SIRAS, single isomorphous replacement with anomalous scattering.

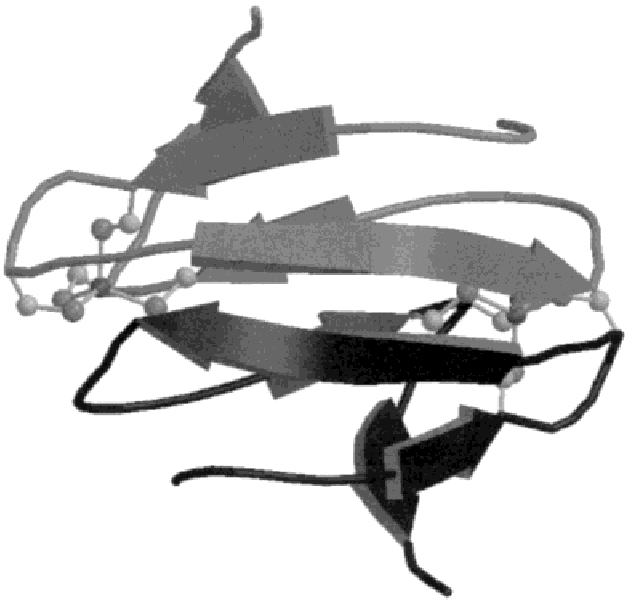

Fig. 1. Ribbon diagram of the Dx calculated with program MOLSCRIPT (Kraulis, 1991) and RASTER-3D (Merritt & Murphy, 1994). Both iron atoms are represented as spheres with the coordinating cysteines. View along the molecular dyad axis.

rubredoxin-like centers have also been found in larger proteins, in association with other iron sites, providing unique combinations of metal centers. These include desulfoferrodoxin (Dfx), rubrerythrin (Rr), and nigerythrin (Moura et al., 1994, 1999). Rr was isolated from *Desulfovibrio desulfuricans* ATCC 27774 and *Desulfovibrio vulgaris* (Hildenborough) as a homodimer of 44 kDa (Pierik et al., 1993). The crystallographic structure of *D. vulgaris* Rr (deMaré et al., 1996) shows that each monomer is composed of two domains. The first domain with 146 amino acid residues is similar to hemerythrin, while the second domain resembles Rd in terms of the $Fe(SCys)_4$ center and the domain folding, which is partially superimposable to Rd (deMaré et al., 1996). In Dfx, a single polypeptide chain of 13.9 kDa provides the ligands for two iron centers in the molecule. One is similar to the center of Dx, while the second center is of the type $Fe[(SCys)\ (NHis)_4]$. Dfx from *D. desulfuricans* (Coelho et al., 1997) is a crystallographic homodimer and its N-terminal domain is superimposable to the Dx dimer with an RMSD of 0.59 Å for all main-chain atoms.

Metal replacements are easily carried out with Rd and Dx via reconstitution of the apoprotein with the appropriate metal salts (Moura et al., 1991; Archer et al., 1995; Ayhan et al., 1996). The derivative containing Ni^{2+} is of particular interest, as Ni substituted Rd and Dx were shown to mimic the reactivity pattern of Ni-containing hydrogenases with respect to hydrogen production, deuterium-proton exchange, and inhibition by carbon monoxide (Saint-Martin et al., 1988), and represent a structurally homologous fragment of the Ni-Fe site in bacterial hydrogenases (Volbeda et al., 1995). However, while in Dx the coordination seems to be a distorted tetragon, in the Ni-Fe hydrogenases it is a square planar.

During the overexpression of the recombinant proteins (Dx and Rd), *Escherichia coli* produces Zn and Fe isomorphs (Eidsness et al., 1992; Petillot et al., 1993; Czaja et al., 1995). Speculations were made about whether the Zn incorporation was an artifact of the heterologous expression in *E. coli* (Petillot et al., 1993) or whether their presence had simply not yet been detected during purification from the native host. To get a better understanding of the mechanisms that are responsible for the incorporation of different metals into the metal site of proteins, several experiments have been reported. Proton titrations were performed to evaluate the affinity of different metals to the Dx metal site, as protons compete with the metal for protein ligands (Kennedy et al., 1998). In that study Fe^{3+} bound most tightly. The relative affinity for Cd^{2+} and Zn^{2+} was determined to be $Zn^{2+} > Cd^{2+}$ for wild-type Dx and for a polypeptide corresponding to the N-terminus domain of Dfx. Cd^{2+} bound tighter than Zn^{2+} in two Dx mutant proteins, for which one or two residues have been inserted between the vicinal cysteines. Moreover, the results seem to indicate that metal dissociation appears to occur in a single cooperative step involving four protons. Other studies were done involving direct metal substitution at the *Clostridium pasteurianum* Rd $M(SCys)_4$ site (Bonomi et al., 1998). Addition of a modest molar excess of Cd^{2+} and Zn^{2+} was shown to displace the Fe^{2+} in reduced Rd under anaerobic conditions without protein denaturants. Moreover, Fe^{2+} could not be reinserted in Cd and Zn substituted Rd. Under similar conditions, Cd^{2+} could substitute for Zn^{2+}, thereby indicating the relative metal affinities of $Cd^{2+} > Zn^{2+} > Fe^{2+}$. On the contrary, Ni^{2+}, Co^{2+}, or VO^{2+} salts could not displace Fe^{2+}. The metal substitutions were proposed to occur without unzipping the β-sheet or unfolding of the structure. Similar to Dx, the incubation with divalent metals produced no substitution of oxidized Fe^{3+} Rd, which is very stable.

This paper reports the crystallization and X-ray diffraction analysis of Dx replaced with different metals, in particular In^{3+}, Ga^{3+}, Cd^{2+}, Hg^{2+}, and Ni^{2+} (preliminary analysis) and compares the three-dimensional structures obtained. The replacement of iron in Dx by different metal ions, while following the metal center geometry and the protein folding, is a suitable experiment to test the energized conditions proposed by Vallee and Williams (1968) and Williams (1995).

Results and discussion

Metal reconstitution

The overexpression of the *D. gigas* gene encoding for Dx in *E. coli* enabled a large amount of protein to be purified as described by Czaja et al. (1995). The Zn^{2+} form of recombinant Dx was used to reconstitute the protein with the following metal ions: V^{3+}, Mn^{2+}, Co^{2+}, Ni^{2+}, Zn^{2+}, Cd^{2+}, Hg^{2+}, Ga^{3+}, and In^{3+}—in all cases a stable protein solution was obtained.

Crystallization and preliminary characterization

Crystallization experiments were carried out for all nine metal derivatives, V-, Mn-, Co-, Ni-, Zn-, Cd-, Hg-, Ga-, and In-Dx—in all cases some crystalline material was formed. Good quality three-dimensional crystals were easily obtained for the Fe- native protein, as well as for In- and Ga-Dx. Diffraction quality crystals were also grown for Ni-, Cd-, and Hg-Dx, although a more extensive screen was required for these metal ions. In contrast, crystalline material for the V-, Mn-, Co-, and Zn-Dx proteins was obtained, but they formed small multiple plates, which were unsuitable for diffraction studies.

Crystallization of metal reconstituted Dxs is divided into three space groups. Crystals of In- and Ga-Dx are isomorphous to the native (Fe-Dx) ones and grew under the same or similar experimental conditions. Their crystals are elongated trigonal bipyramids, red brownish for Fe-Dx and colorless for In- and Ga-Dx. These crystals belong to the trigonal space group $P3_221$, with cell parameters $a = b = 42.2$ Å and $c = 72.3$ Å. The calculated V_M for the crystals is 2.4 Å^3/Da, corresponding to approximately 49% of solvent content (Matthews, 1968). The Cd- and Hg-Dx crystals belong to the space group $P3_121$, with cell dimensions $a = b = 27.9$ Å and $c = 130.9$ Å. Colorless hexagonal plates were grown in a buffered solution (pH about 5) containing ethanol as precipitant and Ca^{2+}. Ni-Dx crystals (yellow bi-dimensional plates), grown in PEG 4K at a more basic pH (about 7.5) crystallized in space group C2, with $a = 47.2$ Å, $b = 30.2$ Å, $c = 84.1$ Å, and $\beta = 97.1°$. The Cd-, Hg-, and Ni-Dx crystals have a V_M of 1.9 Å^3/Da with a solvent content near 35%. This indicates the presence of one dimer in the asymmetric unit for Cd- and Hg-Dx, and two dimers in the asymmetric unit of the Ni-Dx crystals.

Complete data sets for Ga-, Cd-, and Hg-Dx were collected from one single crystal. For Ni-Dx, three crystals were measured, but the merging of the diffraction data only achieved an overall completeness of 81%. There was a cuspid of data, around 20%, which could not be measured because this lack of data corresponded to the thinnest dimension of the Ni-Dx yellow plates, as these crystals were almost bi-dimensional. Synchrotron radiation data might ensure a better data set.

Structure solutions and refinements

The Ga-Dx structure was solved by difference Fourier methods using the Fe-Dx coordinates without solvent molecules as a model, since Ga-Dx and native (Fe-Dx) crystals are isomorphous. The structures of Cd-, Hg-, and Ni-Dx derivatives were solved by molecular replacement methods with AMoRe (Navaza, 1994), using the Fe-Dx structure as a search model. The crystal structures of Ga-, Cd-, and Hg-Dx were refined to 1.9, 2.0, and 2.5 Å resolution, respectively (Table 1). The refinement of the Hg-Dx structure was performed with X-PLOR (Brünger, 1992). The final *R*-factor is 18.2% for all data above 2σ. Crystallographic refinements of Ga- and Cd-Dx structures were done with SHELX-97 (Sheldrick & Schneider, 1997) using all data to an *R*-factor of 17.9 and 18.9%, respectively.

Although for the Ni-Dx crystals the measured data set was not complete, the structure could be solved by molecular replacement. The refinement with two dimers in the asymmetric unit was performed with X-PLOR, using data in the resolution range 10–2.2 Å. Molecular dynamics and positional refinements done on the Fe-Dx model without solvent molecules allowed the *R*-factor to drop from 37.2–31.1%. Inspection of the electron density map revealed, as expected, many breaks throughout the protein polypeptide chain. The averaged electron density map calculated with SigmaA (CCP4, 1994) was considerably improved. In one of the Ni-Dx monomers, the density around the metal site was particularly well defined. This density suggested that in this metal derivative as well the geometry is tetrahedral. Due to the lack of diffraction data, this structure was not refined further and will not be included in the discussion on the structural analysis of the different metal substituted Dx.

Primary sequence homology

A search in the Swissprot Database for homologous amino acid sequences of Dx was performed with the Blast server (Altschul et al., 1990). The highest scores were obtained for Dfx. The sequence alignment done with CLUSTAL W (Thompson et al., 1994) between *D. gigas* Dx and the N-terminal domain (the first 36 amino acids) of Dfx isolated from *D. vulgaris* (strains Hildenborough and Miyazaki) and *D. desulfuricans* showed 54 and 48% identity, respectively (Fig. 2).

Interestingly, the N-terminal domains of several neurophysin molecules show a pattern of cysteine residues similar to Dx, e.g., Cys10-X-X-Cys13-Gly14–[13X]–Cys27-Cys28-Gly29- for bovine neurophysin vs. Cys9-X-X-Cys12-Gly–[11X]–Cys28-Cys29-Gly30- for Dx. Neurophysin is a carrier protein of the pituitary hormone oxytocin. The crystallographic structures of the bovine

Table 1. *Model quality and refinement statistics*

	Ga-Dx	Cd-Dx	Hg-Dx
Total number of non-H atoms	587	577	538
Number of solvent molecules	60 (one sulfate)	53	14
Temperature factors (Å^2)			
Main chain	18.6	18.7	43.5
Side chain	27.3	26.2	48.5
Solvent molecules	44.3	29.5	36.9
RMSD			
Bond lengths (Å)	0.008	0.005	0.009
Bond angles[a] (Å, °)	0.026	0.018	1.61
Dihedrals (°)			25.9
Impropers (°)			0.98
Overall *R*-factor	0.179	0.189	0.182
(Resolution range (Å))	(25.7–1.9)	(14.8–2.0)	(23.5–2.5)
Refinement program	SHELXL-97	SHELXL-97	X-PLOR

[a]SHELX-97 outputs the RMSD of bond lengths in Å (distances 1,3).

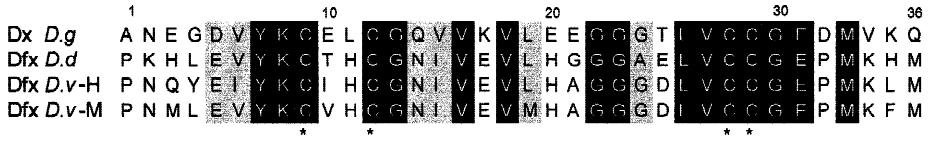

Fig. 2. Multiple amino acid sequence alignment using CLUSTAL W (Thompson et al., 1994) of Dx with the N-terminii of Dfxs from *D. vulgaris* strains Hildenborough, from Miyazaki, and from *D. desulfuricans*, which showed 54, 48, and 48% identity, respectively. The cysteine residues bound to the iron atom are shown with an asterisk.

neurophysin and its complex with the oxytocin hormone have been determined (Chen et al., 1991; Rose et al., 1996). It is a dimeric protein (about 2×10 kDa) containing 14 cysteine residues, all of them involved in disulfide bridges, which help in stabilizing the overall structure. The monomer structure consists of two domains, each forming four-stranded antiparallel β-sheets connected by one 3_{10}-helix and a loop. Although the Cys ligating pattern (Cys-X-X-Cys-Gly–[X_n]–Cys-Cys-Gly) is similar in the bovine neurophysin and Dx, the structural arrangements of the corresponding peptide segments in both structures are totally different. This example is the opposite of Dx and Dfx N-terminus, where similar amino acid sequences fold into nearly identical three-dimensional structures, the difference being the absence of a (structural) metal ion in the neurophysin molecule.

Desulforedoxin and rubredoxin

Dx and Rd show structural similarity for segments comprising Tyr7 to Val16, and Met33 to Gln36 (Dx numbering scheme), for which the superposition of all main-chain atoms gives an RMSD of 1.45 Å (Fig. 3). This conserved region in both structures includes the first pair of cysteine residues. To the contrary, the other pair of vicinal cysteines (Cys28–Cys29) in Dx imposes a different polypeptide conformation when compared to Rd.

As a consequence of the different Cys chelating motif both proteins exhibit a different NH–S bonding pattern. These bonds may contribute to the stabilization of the metal center by accommodating the metal ion without creating strain in the protein conformation (Adman et al., 1975). These interactions are thought to be important for the determination of redox potential and function (Sheridan et al., 1981; Backes et al., 1991). The Dx center has an unsymmetrical pattern with four H-bonds (Fig. 4A). The NH–S bonding pattern for Rd, being approximately twofold symmetrical, is different from Dx (Fig. 4B) and involves a total of six NH–S bonds.

In respect to the water structure of both proteins, in Dx there are two hydrogen bonded buried water molecules (W27 and W28 in Fig. 4A). These two waters may be important for mediating electron transfer, in contrast to Rd where no internal waters have been described. The innermost water is 5 Å away from the iron atom and is within hydrogen bonding distance from the sulfur atom of Cys9 and from the carbonyl oxygen atom of Cys28, leading to solvent accessibility to the metal. The active sites of both Rd and Dx are exposed at the surface of the protein molecule and ready to interact with a redox partner. Therefore, direct electron transfer to the metal center must occur rapidly and without the involvement of long-range electron transfer.

Comparison of different metal derivative structures

The metal coordination geometry for the different Dx metal substituted derivatives is presented in Table 2. The most significant differences among them are the increased metal-SCys bond lengths, which follow the trend expected for these ionic metal radii. In the native Dx and Rd structures, the Fe-S bond distances are in agree-

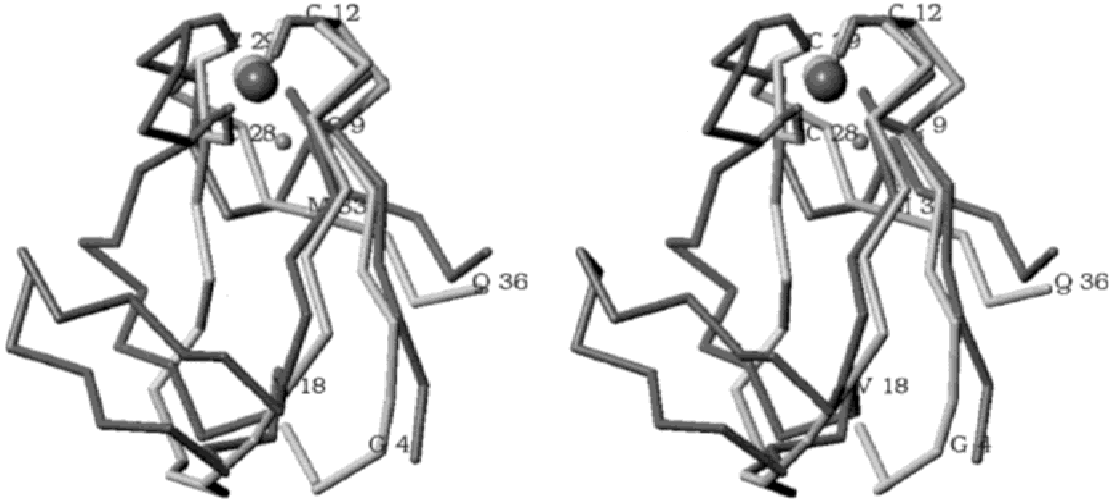

Fig. 3. Stereoscopic Cα superposition of *D. gigas* Rd (dark gray) with one Dx monomer (light gray), showing a conserved region for segments 4–18 ("rubredoxin knuckle") and 33–36 (Dx numbering).

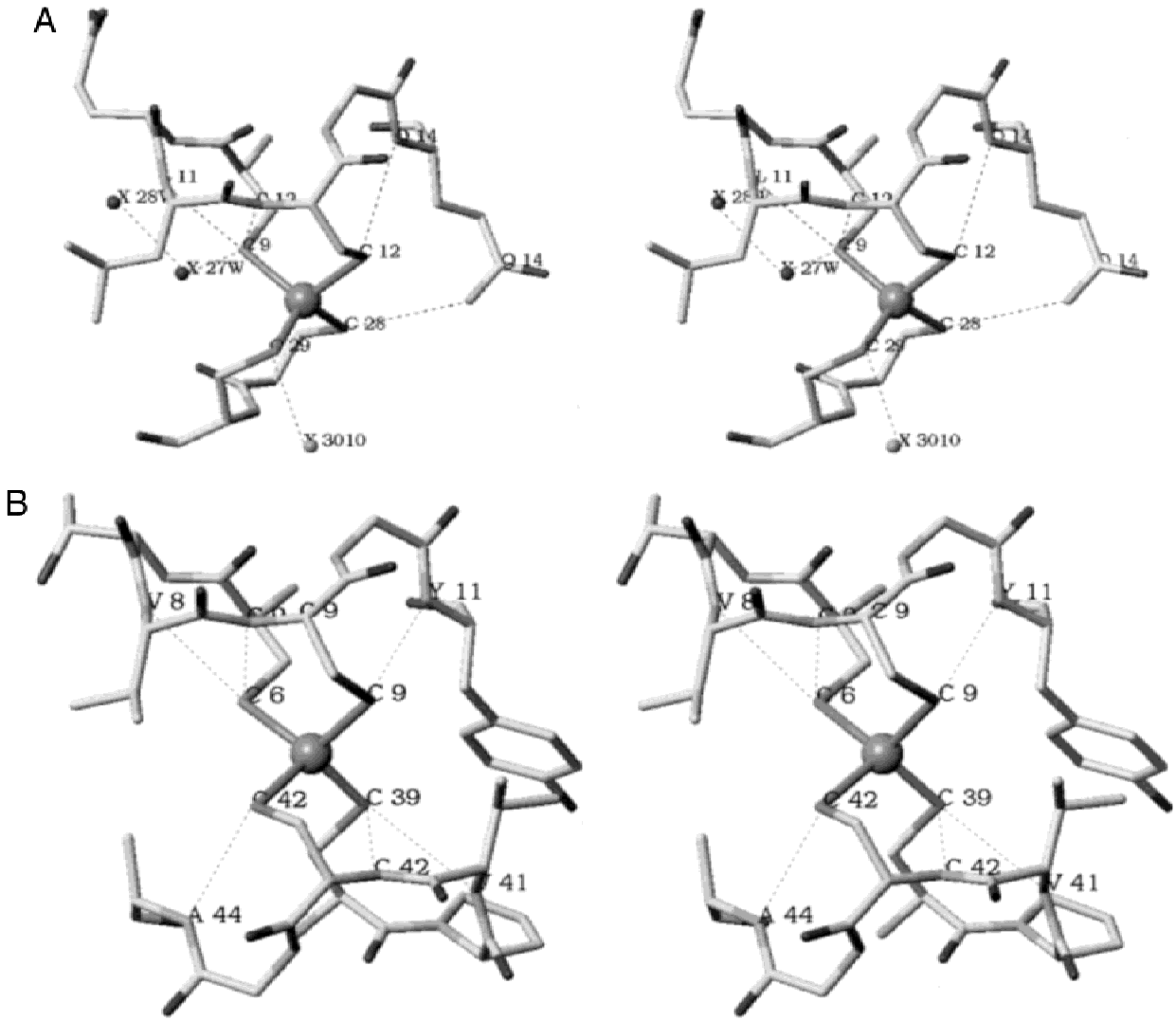

Fig. 4. A: Stereo view of the Dx $Fe(SCys)_4$ center with NH–S bonds marked (dashed line). NH–O bonds with two conserved water molecules, 27W and 28W, observed in all metal-replaced Dx structures and another water molecule, 3010, only observed for the Cd- and Hg-Dx structures, are also shown. **B:** Stereo view of the *D. gigas* Rd $Fe(SCys)_4$ center viewed along the pseudo twofold axis, with NH–S hydrogen bonds marked (dashed line). The orientation is approximately the same as that in **A** for the Dx center.

ment with those found in some model compounds (Lane et al., 1977; Millar et al., 1996). There are deviations from the tetrahedral coordination with enlargement of the (Cys28)Sγ -M- Sγ(Cys29) bond angle (mean values of 120.2–123.8°). This is in contrast to Rd where all angles are close to a tetrahedral arrangement either in the native, or in the metal replaced rubredoxins, such as Zn-Rd (Dauter et al., 1996) or Cd-Rd (Ayhan et al., 1996). In all metal substituted Dx and Rd, the typical network of NH–S hydrogen bonds is maintained in the MS_4 core, but with some differences in the respective bond lengths. The most significant differences are found for the Cd-Dx, as well as in Cd-Rd (Ayhan et al., 1996) in comparison to the native structures. As a consequence of the larger metal core, there is a decrease in the NH–S distances to the most buried cysteines (Cys9 in Dx, Cys6 and Cys39 in Rd). As might be expected, differences around the metal site may also influence the hydrogen bonding pattern of the Cys28–Cys29 loop. In the native Fe-Dx, as well as in the isomorphous In- and Ga-Dx ($P3_221$), the S^{γ} of the most exposed cysteine residue (Cys29) establishes no NH–S hydrogen bonds although it contacts a close sulfate molecule from the crystallization buffer. In the $P3_121$ packing of Hg- and Cd-Dx, the intermolecular contacts are looser. In these structures, Cys29 is hydrogen bonded through its sulfur atom to a water molecule with a S–OH distance of 2.8 Å (W3010 conserved in the two structures and in subunits A and B) (Fig. 4A). Concerning the solvent network, some variations are observed among the structures. The refined models of Ga-, Cd-, and Hg-Dx include 59, 53, and 14 water molecules, respectively. All water molecules are found at the periphery of the Dx molecule, with the exception of two internal water molecules near the metal site (W27 and W28), which are conserved in all metal substituted Dx structures, and a more exposed water, only found in the Cd- and Hg-Dx structures (W3010).

Similar to Fe- and In-, the Ga-Dx model also contains a sulfate ion due to the use of lithium sulfate as precipitant. The Cd- and

Table 2. *Comparison of metal coordination geometry in different metal-substituted desulforedoxins*

(Mean values)[a]	Fe-Dx[b]	In-Dx[b]	Ga-Dx[c]	Cd-Dx[c]	Hg-Dx[c]
Bond distances (Å)					
M–Sγ C9	2.29	2.45	2.27	2.53	2.56
M–Sγ C12	2.32	2.45	2.24	2.54	2.56
M–Sγ C28	2.30	2.46	2.28	2.55	2.57
M–Sγ C29	2.30	2.47	2.24	2.55	2.63
Bond angles (°)					
C9 Sγ–M–Sγ C12	109.4	107.9	111.6	106.5	107.9
C9 Sγ–M–Sγ C28	108.2	106.0	107.6	110.0	106.4
C9 Sγ–M–Sγ C29	110.7	109.8	109.5	103.2	104.4
C12 Sγ–M–Sγ C28	103.2	104.3	102.2	109.2	115.6
C12 Sγ–M–Sγ C29	103.8	104.3	105.6	105.0	101.5
C28 Sγ–M–Sγ C29	121.8	123.8	120.6	120.8	120.2
Hydrogen bonds (Å)					
NH–S					
L11 NH–Sγ C9	3.54	3.59	3.53	3.36	3.44
C12 NH–Sγ C9	3.51	3.51	3.50	3.42	3.56
Q14 NH–Sγ C12	3.67	3.74	3.59	3.60	3.61
Q14 Nε2–Sγ C28	3.50	3.40	3.46	3.52	3.57
OH–S					
(Water) OH–Sγ C9	3.27	3.21	3.26	3.44	
(Water) OH–Sγ C29				2.78	2.84

[a] Average distance or angle values of both Dx subunits.
[b] Archer et al. (1995).
[c] This paper.

Hg-Dx models have a network of hydrogen bonded water molecules instead of the sulfate ion, as also happens for the native structure (Archer et al., 1995). There are seven well-ordered water molecules, which mediate in different ways the intermolecular contact between the two monomers, contributing to the stability of the Dx dimer. These structural water molecules are conserved in all metal replaced Dxs, despite the different crystallization conditions. The different packing symmetries $P3_121$ and $P3_221$ also imply a different water structure in crystal contact regions for the two space groups. In the two different packing modes, the cell with symmetry $P3_221$ brings the metal atoms from symmetry related molecules only 8 Å apart, while in the $P3_121$ case the closest distance between the Cd (or Hg) atoms of symmetry mates is about 16 Å. Probably due to the different packing, in the Cd- and Hg-Dx structures there is a water molecule (W3010) that makes an H-bond to the Sγ from Cys29, mediating the contact through two additional waters to Glu10 and Lys8 of a symmetry related molecule.

The overall folding of the different metal substituted structures (In^{3+}, Ga^{3+}, Cd^{2+}, and Hg^{2+}) when compared to the native structure (Fe^{3+}) are quite similar. The RMSD with respect to Cα atoms among all structures are given in Table 3. The Cd- and Hg-Dx backbones are the ones that deviate more significantly from the native structure (RMSD for the Cα atoms superposition is around 0.3 Å). As expected, the side chains of some charged amino acid residues located on the molecule surface, e.g., glutamates 3, 10, 20, 31, and lysine 17, along with the N-terminii (first three amino acids) are the most variable regions among the different metal substituted structures (RMSD may go up to 0.6 Å). Comparison of the backbone structures reveals that the replacement of Fe^{3+} by larger metal ions, such as Cd^{2+} or Hg^{2+}, induces more relevant conformational changes near the adjacent cysteines (Cys28, Cys29), namely, in the polypeptide segment comprising residues Val27 to Asp32. In particular, the glycine residues (Gly13 and Gly30) show greater deviations in comparison with neighboring residues (for the Cd-Dx their RMSD is two times higher than the values presented by the other vicinal atoms), suggesting that they can accommodate changes more easily in the surrounding conformation. The backbone of the two residues between the first pair of cysteines (Glu10 and Leu11) also shows some structural rearrangements.

Entatic state of the metal site

According to Williams (1995), there are several ways in which local groups such as an amino acid, a bound metal ion, or a cofactor can be structurally energized by the protein and/or themselves contribute to modifications of the protein structure. One way is when the protein provides a rigid matrix that strains the metal into an unusual, energized state. This was proposed to be the case for zinc in carbonic anhydrase or copper in the blue proteins,

Table 3. *RMSD for the superposition of the Cα atoms of the different metal reconstituted derivatives (Å)*

	Fe-Dx	In-Dx	Ga-Dx	Cd-Dx	Hg-Dx
Fe-Dx	—	0.12	0.14	0.30	0.31
In-Dx	—	—	0.15	0.31	0.32
Ga-Dx	—	—	—	0.29	0.30
Cd-Dx	—	—	—	—	0.20

such as azurin and plastocyanin (Williams, 1995). More recent work raised some doubts against this hypothesis suggesting that the cupric geometry of blue copper proteins is not strained (Ryde et al., 1996). The possibility of replacing the iron ion in Dx by different metal ions followed by an atomic level determination of the protein structure and metal center geometry constitutes a helpful tool to test the entatic state of the metal site. The comparison of the different metal derivatives' three-dimensional structures shows similar overall secondary and tertiary structures. In terms of metal coordination geometry, the tetrahedral arrangement is maintained as should be expected for metals such as Fe^{3+}, In^{3+}, Ga^{3+}, Cd^{2+}, and Hg^{2+}, where an increase of metal-sulfur bond lengths follows the increase of the metal ion ionic radii (Table 2). In these cases, the replacement of metal ions in Dx seems to neither distort the protein folding nor significantly alter the geometry of the metal site. However, the comparison of the metal centers in Dx and Rd shows some differences as expected. In native (Fe^{3+}) and Cd^{2+} substituted Rd (Ayhan et al., 1996), the metal bond lengths are similar to Dx, whereas the angles with the cysteinyl sulfur atoms are closer to tetrahedral (~100.8–114.8°). On the contrary, in Dx, a pronounced enlargement of the Cys28-M-Cys29 angle is observed (120.2–123.8°), caused by the adjacent cysteines. In this respect, two mutants of Dx, where one (Gly) or two residues (Pro-Val) were inserted between these vicinal cysteines, showed similar spectroscopic data to Rd (Yu et al., 1997). These results suggest that the geometry of the bound group, in these cases the metal ion, is enforced by the rigid framework of the protein. To further explore this hypothesis, it would be useful to have the apoprotein structure to determine whether the protein backbone is essentially the same without the metal bound to it.

Summarizing, the $Fe(SCys)_4$ site in Dx and in Rd can incorporate other metal ions (In^{3+}, Ga^{3+}, Cd^{2+}, Ni^{2+}, and Hg^{2+} in Dx, Zn^{2+}, or Cd^{2+} in Rd) without major changes in the protein structure, suggesting that the similar fold and structural arrangement around the metal centers are almost invariant with the metal type. These results seem to be in agreement with the entatic state theory of groups (Vallee & Williams, 1968; Williams, 1995).

Conclusions

The incorporation of a number of metal ions in the $Fe(SCys)_4$ site of Rd or Dx and the availability of some of their three-dimensional structures provide valuable information about significant structural changes at the metal sites. The comparison of the Rd and Dx derivatives substituted with different metals shows that no major changes occur in the overall folding of the protein or near the metal center. Hence, the nearly identical fold of the consensus sequence -Cys-X-X-Cys- or -Cys-Cys- binding motifs does not rely on the chemical nature of the particular metal. The choice of the metal may rather derive from its cellular bioavailability and incorporation into appropriate proteins (Silva & Williams, 1991), rather than from a structural basis. Moreover, the question of why other potential structural metals are not often found may be due to some poisoning effect (e.g., cadmium or mercury) to the cell or to some thermodynamic or kinetic factors that might control the metal incorporation in certain metal binding sites. Thermodynamic control is known to determine the metal incorporation in certain metal binding sites (Hausinger, 1990) and in the case of zinc, it is known that it binds more tightly to thiols than does iron. Therefore, the preference of iron in rubredoxin-type proteins may be determined by the metal natural abundance, as found in the case of *D. gigas* Dx as well as Rd isolated from different bacterial sources, that incorporate exclusively iron. In contrast, in the overexpression of recombinant Rd (Eidsness et al., 1992; Petillot et al., 1993) and Dx (Czaja et al., 1995), *E. coli* produces the zinc along with the iron form.

Additionally, renewed interest in mononuclear centers has emerged since they have been found in association with other metal centers, such as the dioxo-iron center in Rr and the pentacoordinated ferric iron in Dfx. Genetic studies suggest that genes encoding the smallest units containing one iron atom, e.g., Dx and Rd, may fuse to form genes encoding higher molecular weight redox proteins containing several metal centers (Brumlik & Voordouw, 1989; Brumlik et al., 1990).

This structural approach may be just the beginning of a more systematic exploitation of the influence of the change of d-shell electrons on the structure itself, to draw possible correlations with spectroscopic and redox properties of the metal center. Further insight into this problem may benefit from more accurate structural data derived from atomic resolution crystal structures when synchrotron data will be available.

Materials and methods

Protein overexpression and purification

The *dsr* gene from *D. gigas* genomic DNA encoding for Dx has been cloned using the polymerase chain reaction, expressed in *E. coli* and purified to homogeneity as previously described (Czaja et al., 1995).

Metal reconstitution

The Zn^{2+} form of the overexpressed protein in *E. coli* was used for reconstitution with several metals. The following metals ions were employed: V^{3+}, Mn^{2+}, Co^{2+}, Ni^{2+}, Zn^{2+}, Cd^{2+}, Hg^{2+}, Ga^{3+}, and In^{3+}. The metal salts used were either nitrate or chloride. The indium substituted Dx (In-Dx) was used as a control, since the In-Dx derivative had already been prepared and its crystal structure analyzed (Archer et al., 1995). The procedure employed was similar to that previously used to replace iron by indium, with some minor modifications. In this paper, the Zn form of the overexpressed protein was used instead of the native protein. All the metal substituted derivatives are colorless, with the exception of Dx reconstituted with Co^{2+} (Co-Dx), which is pale green, and Ni^{2+} (Ni-Dx), which is yellow. Each mixture was then passed through a Sephadex G-25 Medium NAP-5 column (Pharmacia, Uppsala, Sweden) to remove the excess of reconstitution reagents, using 10 mM Tris-HCl pH 7.6 as elution buffer. These metal substituted derivatives were concentrated in centricons YM3 (Amicon, Beverly, Massachusetts) to a final protein concentration around 8 mg/mL, assuming about 20–30% protein lost during the reconstitution procedure. To remove the excess of Ni^{2+}, the Ni-Dx sample was applied to a DEAE-52 column equilibrated with 10 mM Tris pH 7.5. A discontinuous gradient with NaCl (from 0.01–0.5 M NaCl) in 10 mM Tris pH 7.5 was applied and the protein eluted from 0.15–0.25 M NaCl. Second, the sample was dialyzed on a diaflo against 10 mM Tris pH 7.5, while small amounts of EDTA (final concentration ~ 10 mM) were added. These procedures helped eliminate some traces of Ni^{2+} noticed in the optical spectra (data not shown). The most efficient technique to remove the excess of Co^{2+} and Ni^{2+} was the dialysis of the protein sample against EDTA.

Crystallization and crystal stabilization

The first experimental assays were performed for each metal-substituted derivative using the same crystallization conditions as for the native (Fe-Dx) and indium reconstituted (In-Dx) proteins (Archer et al., 1995). The precipitant was either lithium sulfate (0.75 M), ammonium sulfate (1.5 M), or PEG 4K (10% w/V) in a buffered solution of sodium acetate 0.1 M, pH 4.5. Colorless crystals appeared, reproducibly, at room temperature within a few days for In- and Ga-Dx. No other metal substituted derivatives crystallized under these experimental conditions. Initial screenings were then performed, at 4 and 20 °C, by the vapor diffusion method using different starting crystallization conditions. Equal amounts of protein (~7 mg/mL in 10 mM Tris pH 7.6) and crystallization solutions were used, 2 μL of each. Very small thin plates appeared at ~20 °C, after one week, for Zn-, Mn-, Co-, Ni-, and V-Dx in 25% PEG 4K, 0.1 M Hepes pH 7.5 and 0.2 M $CaCl_2$. Some hexagonal plates grew, at room temperature, in 30% ethanol, 0.1 M sodium acetate pH 4.5 and 0.2 M $CaCl_2$ for Cd- and Hg-Dx. Microcrystals were also observed for Zn- and Ni-Dx in the latter conditions, but they disappeared after several days. Narrower searches were done by varying the protein and precipitant concentrations, precipitant nature (different PEGs or different alcohols), drop composition, type of buffer and pH, and different salts and additives (dioxane, ethyleneglycol, zwitterionic compounds, and detergents). No crystals were grown without the addition of $CaCl_2$ to the crystallization buffer. To obtain suitable diffracting crystals, a large set of different experimental conditions were tried. Macro-seeding was employed to obtain bigger hexagonal plates for Cd- and Hg-Dx, which grew to dimensions of $0.3 \times 0.3 \times 0.15$ mm^3. The Ni-Dx protein yielded yellow bidimensional plates at different temperatures (4, 12, and 20 °C), with propensity to form aggregates or multiple crystals (maximum $0.5 \times 0.3 \times 0.1$ mm^3). Unfortunately, these crystals were not very reproducible and were also dependent on the reconstitution batch. The preliminary crystal characterization is shown in Table 4.

The Ga-Dx crystals grown in ammonium sulfate were harvested by increasing the precipitant (ammonium sulfate) concentration to 1.8 M. Several trials were necessary to stabilize the Cd- and Hg-Dx crystals, grown in ethanol. The addition of glycerol or 2-methyl-2,4-pentanediol (MPD), in the range 20–30%, induced the crystal degradation after about 15 min. However, the addition of 30% PEG 4K (w/V) to the crystallization buffer proved to be a good harvesting buffer (Cd-Dx), also suitable for cryogenic conditions (Hg-Dx). The stabilization of the Ni-Dx crystals, grown in PEG 4K, was achieved by increasing the precipitant concentration to 30% and adding glycerol (5–10%). The crystals (Hg- and Ni-Dx) were soaked briefly in the harvesting buffer prior to flash cooling in the cold nitrogen gas stream, needed for data collection.

Data collection

X-ray diffraction data sets were collected using graphite monochromated Cu-K_α radiation, with a 0.5 mm collimator from a rotating anode generator operated at 5.2 kW (Cd-Dx) or 4.5 kW (Ga-, Hg-, and Ni-Dx). An 18 cm diameter MAR-Research (Hamburg, Germany) imaging plate scanner was used as detector. Diffracting data were processed with the programs Denzo and Scalepack (Otwinowski & Minor, 1995) and Truncate (CCP4, 1994). Some useful statistics to assess the quality of the data are presented in Table 4. Complete data sets for Ga-, Cd-, and Hg-Dx were collected from one single crystal each. For Ni-Dx three crystals were measured, but the merging of the diffraction data led to an overall completeness of only 81% (Table 4).

Structures determination

The Ga-Dx structure was solved by difference Fourier methods using the Fe-Dx coordinates, as Ga- and native crystals (Fe-Dx) are isomorphous. Since Cd-, Hg-, and Ni-Dx crystallize in different space groups (Table 4), their structures were solved by molecular replacement using the Fe-Dx as a search model. AMoRe (Navaza, 1994) gave the same unambiguous solution for Cd- and Hg-Dx, with correlation coefficients of 0.631 and 0.528 (about two times the standard deviation above the mean value) and *R*-factors of 0.358 and 0.419, respectively. The data resolution ranged from 10–3.5 Å. Another solution was found for the dimer with the same correlation coefficient, which corresponded to a rotation of 180°,

Table 4. *Crystal characterization and data processing statistics*

	Ga-Dx	Cd-Dx	Hg-Dx	Ni-Dx[a]
Space group	$P3_221$	$P3_121$	$P3_121$	C2
Cell dimensions (Å)	$a = b = 42.2$, $c = 72.3$	$a = b = 27.9$, $c = 130.9$	$a = b = 27.9$, $c = 130.9$	$a = 47.2$, $b = 30.2$, $c = 84.1$ $\beta = 97.1°$
V_M (Å^3/Da)	2.4 (1 dimer)	1.9 (1 dimer)	1.9 (1 dimer)	1.9 (2 dimers)
Resolution range overall	25.7–1.95	14.8–1.98	23.5–2.50	23.8–2.2
(outer shell) (Å)	(2.04–1.95)	(2.05–1.98)	(2.59–2.50)	(2.31–2.20)
Measured reflections	46,772	28,142	25,156	29,474
Unique reflections (multiplicity)	6,148 (7.6)	4,403 (6.4)	2,199 (11.4)	4,809 (6.1)
Completeness (%) overall				
(outer shell)	98.2 (93.9)	97.5 (96.4)	94.1 (93.1)	~81 (74.3)
$I/\sigma(I)$ overall (outer shell)	12.8 (2.2)	8.0 (2.5)	9.4 (3.2)	7.4 (4.1)
R_{sym}[b] (%) overall (outer shell)	11.8 (36.8)	11.5 (43.2)	10.3 (35.9)	8.2 (15)

[a] Merged data from three different crystals.

[b] $R_{sym}(I) = \sum(|I(k) - \langle I\rangle|)/\sum I(k)$, where $I(k)$ and $\langle I\rangle$ represent the diffraction intensity values of individual measurements and the corresponding mean values. The summation is over all measurements.

i.e., interchange of chain A and B within the dimer structure. The Ni-Dx crystals belong to space group C2, with two dimers in the asymmetric unit. Although the data set for Ni-Dx is not complete, a unique solution was found for the two dimers, showing a correlation coefficient of 0.619 and an *R*-factor of 0.347. The next false solution had a correlation coefficient of 0.407 and an *R*-factor of 0.448. Four equivalent solutions were found for the Ni-Dx structure solution.

Structures refinement

A search in the Cambridge Structural Database (CSD) was performed to infer typical metal distances to the cysteinyl sulfur atoms. Small molecule compounds, for which the metal is coordinated to four sulfur atoms, suggested distances for Ga-, Cd-, and Hg-S of 2.26, 2.54, and 2.57 Å, respectively. Throughout the refinement of all three structures, the metal site geometry was restrained according to the above target values for the metal–sulfur bond distances. The imposed restraints were loosened at the final refinement cycles for the Ga- and Cd-Dx structures. Crystallographic refinements were carried out using the Fe-Dx coordinates without water molecules as a starting model. Rebuilding and addition of solvent molecules were done graphically on a Silicon Graphics workstation and using the program TURBO-FRODO (Roussel & Cambillau, 1989). Refinement of Hg-Dx structure was performed by simulated annealing and/or conventional least-squares refinement with X-PLOR (version 3.1) (Brünger, 1992). The Engh and Huber (1991) force field was used. Restrained noncrystallographic symmetry (NCS) and bulk solvent correction were applied during the refinement procedure. The final *R*-factor is 18.2% for all data above 2σ (to 2.5 Å resolution). Refinement of the Ga- and Cd-Dx structures was done with SHELX-97 (Sheldrick & Schneider, 1997), using the "SWAT" option to model diffuse solvent and local noncrystallographic symmetry restraints were applied. The final *R*-factor is 17.9% for Ga-Dx and 18.9% for Cd-Dx, for resolution ranges of 25.7 to 1.9 and 14.8 to 2.0 Å, respectively. A Ramachadran plot of metal substituted Dx structures shows that all nonglycine residues lie within the allowed regions. The final refinement statistics and model quality parameters are listed in Table 1.

The refinement using the correctly positioned Fe-Dx model (without solvent molecules) within the Ni-Dx crystal unit cell was done with X-PLOR for two dimers in the Ni-Dx asymmetric unit. Simulated annealing using molecular dynamics was done in conjunction with positional energy minimization (Brünger, 1992) and the *R*-factor decreased from 37.2–31.1%, using data in the resolution range 10–2.2 Å. An averaged electron density map was calculated with SigmaA (CCP4, 1994), which revealed many breaks throughout the protein polypeptide chain and therefore no model building was carried out. A complete data set is needed to proceed with further crystallographic refinement.

The atomic coordinates have been deposited in the Brookhaven Protein Structure Database with the accession codes 1dcd, 1cfw, and 1dhg, for DxCd, DxGa, and DxHg, respectively.

Acknowledgments

MA and ALC thank Fundação para a Ciência e Tecnologia for PhD grants (PRAXIS/BD/2795/94 and PRAXIS/BD/15763/98). FR was a PRAXIS XXI Invited Scientist at FCT-UNL. This work was supported in part by the EC Programme BIO4-CT96-0413.

References

Adman ET, Watenpaugh KD, Jensen LH. 1975. NH-S hydrogen bonds in *Peptococcus aerogenes* ferredoxin, *Clostridium pasteurianium* rubredoxin and *Chromatium* high potential iron protein. *Proc Natl Acad Sci USA 72*:4854–4858.

Altschul SF, Gish W, Miller W, Myers EW, Lipman DJ. 1990. Basic local alignment search tool. *J Mol Biol 215*:403–410.

Archer M, Huber R, Tavares P, Moura I, Moura JJG, Carrondo MA, Sieker LC, LeGall J, Romão MJ. 1995. Crystal structure of desulforedoxin from *Desulfovibrio gigas* determined at 1.8 Å resolution: A novel non-heme iron protein structure. *J Mol Biol 251*:690–702.

Ayhan M, Xiao Z, Lavery MJ, Hamer AM, Nugent KW, Scrofani SDB, Guss M, Wedd AG. 1996. The rubredoxin from *Clostridium pasteurianum*: Mutation of the conserved glycine residues 10 and 43 to alanine and valine. *Inorg Chem 35*:5902–5911.

Backes G, Mino Y, Löhr TM, Meyer TE, Cusanovich MA, Sweeney WV, Adman ET, Sanders-Löhr J. 1991. The environment of Fe_4S_4 clusters in ferredoxins and high-potential iron proteins. New information from X-ray crystallography and resonance raman spectroscopy. *J Am Chem Soc 113*:2055–2064.

Bonomi F, Iametti S, Kurtz DM Jr, Ragg EM, Richie KA. 1998. Direct metal ion substitution at the $[M(SCys)_4]^{2-}$ site of rubredoxin. *JBIC 3*:595–605.

Brumlik MJ, LeRoy G, Bruschi M, Voordouw G. 1990. The nucleotide sequence of *Desulfovibrio gigas* desulforedoxin gene indicates that the *Desulfovibrio vulgaris rbo* gene originated from a gene fusion event. *J Bacteriol 172*:7289–7292.

Brumlik MJ, Voordouw G. 1989. Analysis of the transcriptional unit encoding the genes for rubredoxin (*rub*) and a putative rubredoxin oxido-reductase (*rbo*) in *Desulfovibrio vulgaris* Hildenborough. *J Bacteriol 171*:4996–5004.

Brünger AT. 1992. *X-PLOR (version 3.1). A system for X-ray crystallography and NMR*. New Haven, Connecticut: Yale University Press.

Capozzi F, Ciurli S, Luchinat C. 1998. Coordination sphere versus protein environment as determinants of electronic and functional properties of iron-sulfur proteins. In: Hill HAO, Sadler PJ, Thompson AJ, eds. *Structure and bonding—Metal sites in proteins and models—Redox centers*. Berlin, Heidelberg, New York: Springer-Verlag. pp 127–160.

CCP4. Collaborative Computational Project Number 4. 1994. The CCP4 suite: Programs for protein crystallography. *Acta Crystallogr D50*:760–763.

Chen LQ, Rose JP, Breslow E, Yang D, Chang WR, Furey WF Jr, Sax M, Wang BC. 1991. Crystal structure of a bovine neurophysin II dipeptide complex at 2.8 Å determined from the single wavelength anomalous scattering signal of an incorporated iodine atom. *Proc Natl Acad Sci USA 88*:4240–4244.

Coelho AV, Matias P, Fülöp V, Thompson A, Gonzalez A, Carrondo MA. 1997. Desulfoferrodoxin structure determined by MAD phasing and refinement to 1.9 Å resolution reveals a unique combination of a tetrahedral FeS_4 center with a square pyramidal $FeSN_4$ center. *JBIC 2*:680–689.

Czaja C, Litwiller R, Tomlinson AJ, Naylor S, Tavares P, LeGall J, Moura JJG, Moura I, Rusnak F. 1995. Expression of *Desulfovibrio gigas* desulforedoxin in *Escherichia coli*. Purification and characterization of mixed metal isoforms. *J Biol Chem 270*:20273–20277.

Dauter Z, Wilson KS, Sieker LC, Moulis JM, Meyer J. 1996. Zinc- and iron-rubredoxins from *Clostridium pasteurianum* at atomic resolution: A high precision model of a ZnS4 coordination unit in a protein. *Proc Natl Acad Sci USA 93*:8836–8840.

deMaré F, Kurtz DM Jr, Nordlund P. 1996. The structure of *Desulfovibrio vulgaris* rubrerythrin reveals a unique combination of rubredoxin-like FeS4 and ferritin-like diiron domains. *Nat Struct Biol 3*:539–546.

Eidsness MK, O Dell SE, Kurtz DM, Robson RL, Scott RA. 1992. Expression of a synthetic gene coding for the amino acid sequence of *Clostridium pasteurianum* rubredoxin. *Protein Eng 5*:367–371.

Engh R, Huber R. 1991. Accurate bond and angle parameters for X-ray protein structure refinement. *Acta Crystallogr A47*:392–400.

Gomes CM, Silva G, Oliveira S, LeGall J, Liu MY, Xavier AV, Rodrigues-Pousada C, Teixeira M. 1997. Studies on the redox centers of the terminal oxidase from *Desulfovibrio gigas* and evidence for its interaction with rubredoxin. *J Biol Chem 272*:22502–22508.

Goodfellow BJ, Rusnak F, Moura I, Domke T, Moura JJG. 1998. NMR determination of the global structure of the ^{113}Cd derivative of desulforedoxin: Investigation of the hydrogen bonding pattern at the metal center. *Protein Sci 7*:928–937.

Goodfellow BJ, Tavares P, Romão MJ, Czaja C, Rusnak F, LeGall J, Moura I, Moura JJG. 1996. The solution structure of desulforedoxin, a simple iron-sulfur protein. An NMR study of the zinc derivative. *JBIC 1*:341–354.

Hausinger RP. 1990. Mechanisms of metal ion incorporation into metalloproteins. *Biofactors 2*:179–184.

Kennedy M, Yu L, Lima MJ, Czaja C, Moura I, Moura JJG, Rusnak F. 1998.

Metal binding to the tetrathiolate motif of desulforedoxin and related polypeptides. *JBIC 3*:643–649.
Kraulis PJ. 1991. MOLSCRIPT: A program to produce both detailed and schematic plots of protein structures. *J Appl Crystallogr 24*:946–950.
Lane RW, Ibers JA, Frankel RB, Papaefthymiou GC, Holm RH. 1977. Synthetic analogues of the active sites of iron-sulfur proteins, 14.[1] synthesis, properties, and structures of bis(o-xylyl-α,α'-dithiolato)ferrate(II,III) anions, analogues of oxidized and reduced rubredoxin sites. *J Am Chem Soc 99*:84–98
Lovenberg W, Sobel BE. 1965. Rubredoxin: A new electron transfer protein from *Clostridium pasteurianum*. *Proc Nat Acad Sci USA 54*:193–199.
Matthews BW. 1968. Solvent content of protein crystals. *J Mol Biol 245*:54–68.
Merritt EA, Murphy MEP. 1994. Raster3D version 2.0—A program for photorealistic molecular graphics. *Acta Crystallogr D50*:869–873.
Millar M, Lee JF, O Sullivan T, Koch SA, Fikar R. 1996. Models for the iron-sulfur protein rubredoxin: The use of sterically hindered thiolate ligands to stabilize $[Fe(SR)_4]^{-1}$ complexes; some considerations of the structure of the $[Fe(S\text{-}Cys)_4]$ centers in oxidized rubredoxins. *Inorg Chim Acta 243*:333–343.
Moura I, Bruschi M, LeGall J, Moura JJG, Xavier AV. 1977. Isolation and characterization of desulforedoxin, a new type of nonheme iron protein from *Desulfovibrio gigas*. *Biochem Biophys Res Commun 75*:1037–1044.
Moura I, Pereira A, Tavares P, Moura JJG. 1999. Simple and complex iron-sulfur proteins in sulfate reducing bacteria. In: Sikes AG, Cammack RC, eds. *Advances in inorganic chemistry*. Academic Press. In press.
Moura I, Tavares P, Ravi N. 1994. Characterization of three proteins containing multiple iron sites: Rubrerythrin, desulfoferrodoxin, and a protein containing a six-iron cluster. *Methods Enzymol 243*:216–240.
Moura I, Teixeira M, LeGall J, Moura JJG. 1991. Spectroscopic studies of cobalt and nickel substituted rubredoxin and desulforedoxin. *J Inorg Biochem 44*:127–139.
Navaza J. 1994. AMoRe: An automated package for molecular replacement. *Acta Crystallogr A50*:157–163.
Otwinowski Z, Minor W. 1995. *The HKL manual*. New Haven, Connecticut: Yale University Press.
Peterson JA, Kusunose M, Kusunose E, Coon MJ. 1967. Enzymatic omega-oxidation. II. Function of rubredoxin as the electron carrier in omega-hydroxylation. *J Biol Chem 242*:4334–4340.
Petillot Y, Forest E, Mathieu I, Meyer J, Moulis JM. 1993. Analysis, by electrospray ionization mass spectrometry, of several forms of *Clostridium pasteurianum* rubredoxin. *Biochem J 296*:657–661.
Pierik AJ, Wolbert RB, Portier GL, Verhagen MF, Hagen WR. 1993. Nigerythrin and rubrerythrin from *Desulfovibrio vulgaris* each contain two mononuclear iron centers and two dinuclear iron clusters. *Eur J Biochem 212*:237–245.
Rose JP, Wu CK, Hsiao CD, Breslow E, Wang BC. 1996. Crystal structure of the neurophysin-ocytocin complex. *Nat Struct Biol 3*:163–169.
Roussel A, Cambillau C. 1989. *Turbo-frodo in silicon graphics geometry partners directory*. Silicon Graphics Mountain View, California: Silicon Graphics.
Ryde U, Olsson MHM, Pierloot K, Roos BO. 1996. The cupric geometry of blue copper proteins is not strained. *J Mol Biol 261*:586–596.
Saint-Martin P, Lespinat PA, Fauque G, Berlier Y, LeGall J, Moura I, Teixeira M, Xavier AV, Moura JJG. 1988. Hydrogen production and deuterium-proton exchange reactions catalyzed by *Desulfovibrio* Ni(II) substituted rubredoxins. *Proc Natl Acad Sci USA 85*:9378–9380.
Santos H, Fareleira P, Xavier AV, Chen L, Liu MY, LeGall J. 1993. Aerobic metabolism of carbon reserves by the "obligate anaerobe" *Desulfovibrio gigas*. *Biochem Biophys Res Commun 195*:551–557.
Sheldrick GM, Schneider TR. 1997. SHELX: High-resolution refinement. *Methods Enzymol 277*:319–344.
Sheridan RP, Allen LC, Carter CW Jr. 1981. Coupling between oxidation state and hydrogen bond conformation in high potential iron-sulfur protein. *J Biol Chem 256*:5052–5057.
Sieker LC, Stenkam RE, LeGall J. 1994. Rubredoxin in crystalline state. *Methods Enzymol 243*:203–216.
Silva JJRF, Williams RJP. 1991. Zinc: Lewis acid catalysis and regulation. *The biological chemistry of the elements—The inorganic chemistry of life*. New York: Oxford University Press. pp 299–318.
Thompson JD, Higgins DG, Gibson TJ. 1994. CLUSTAL W: Improving the sensitivity of progressive multiple sequence alignment through sequence weighting, position-specific gap penalties and weight matrix choice. *Nucleic Acids Res 22*:4673–4680.
Vallee BL, Williams RJP. 1968. Metalloenzymes: The entatic nature of their active sites. *Proc Natl Acad Sci USA 59*:498–505.
Volbeda A, Charon MH, Piras C, Hatchikian EC, Frey M, Fontecilla-Camps JC. 1995. Crystal structure of the nickel-iron hydrogenase from *Desulfovibrio gigas*. *Nature 373*:580–587.
Williams RJP. 1995. Energized (entatic) states of groups and of secondary structures in proteins and metalloproteins. *Eur J Biochem 234*:363–381.
Yu L, Kennedy M, Czaja C, Tavares P, Moura JJG, Moura I, Rusnak F. 1997. Conversion of desulforedoxin into a rubredoxin center. *Biochem Biophys Res Commun 231*:679–682.